DOI:
10.1021/acs.jpcb.1c03929

Document Version
Peer reviewed version

On the Structure and Flip-flop of Free Docosahexaenoic Acid in a Model Human Brain Membrane

Sze May Yee* and Christian D. Lorenz*

Department of Physics, King's College London, London WC2R 2LS, United Kingdom

E-mail: sze.yee@kcl.ac.uk; chris.lorenz@kcl.ac.uk

Abstract

Among the omega-3 fatty acids, docosahexaenoic acid (DHA, $sn22{:}6$) is particularly vital in human brain cell membranes. There is considerable interest in DHA because low level DHA has been associated with declined cognitive function and poor visual acuity. In this work, atomistic molecular dynamics simulations were used to investigate the effects of free protonated DHA (DHAP) in molar fractions of 0%, 17%, 30% and 38% in a realistic model of a healthy brain cell membrane comprising 26 lipid types. Numerous flip-flop events of DHAP were observed and categorised as successful or aborted. Novel use of the machine learning technique, Density-Based Spatial Clustering of Applications with Noise (DBSCAN), effectively identified flip-flop events by way of clustering. Our data show that increasing amounts of DHAP in the membrane disorders the bilayer packing, fluidises the membrane, as well as increases the rates of successful flip-flop from $k = 0.2\ \mu s^{-1}$ (17% DHAP) to $0.8\ \mu s^{-1}$ (30% DHAP), and to $1.3\ \mu s^{-1}$ (38% DHAP). In addition, we also provided a detailed understanding of the flip-flop mechanism of DHAP across this complex membrane. Interestingly, we noted the role of hydrogen bonds in two distinct coordinated flip-flop phenomena between two DHAP molecules: double flip-flop and assisted flip-flop. Understanding the effects of various concentrations of DHAP on the dynamics within a lipid membrane and the resulting structural properties of the membrane are important when considering the use of DHAP as a dietary supplement or as a potential therapeutic.

Graphical TOC Entry

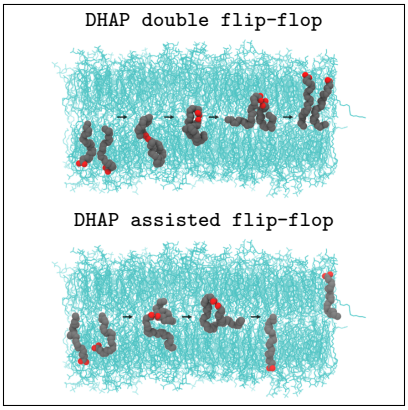

Keywords

docosahexaenoic acid, brain membrane, molecular dynamics, flip-flop, machine learning, DBSCAN

Introduction

Omega–3 fatty acids are known to promote clear benefits in human health, being regarded as essential in brain development,[1–3] in the prevention of Alzheimer's disease[4,5] and also schizophrenia, obesity, hypertension, coronary heart disease, atherosclerosis, and cancer.[5] Docosahexaenoic acid (DHA) is an example of an omega–3 fatty acid (or an n–3 polyunsaturated fatty acid (n–3 PUFA)) that is generally consumed in low amounts in the western diet.[6,7] Dietary DHA supplementation has been demonstrated to have positive impacts on cardiovascular and inflammatory endpoints for a range of metabolic diseases.[8–14] More recently DHA is being investigated as a preventative and therapeutic agent against COVID-19.[15,16]

DHA has also been shown to be essential for brain development, learning and vision. DHA has been shown to accumulate rapidly during the perinatal period and during the first two years of life.[7,17] In addition to its role in the development of the brain, the deficiency of DHA has been linked to many neurodegenerative disorders. As a result, DHA has been investigated as a potential preventative agent against several diseases of the nervous system including depression, epilepsy, Alzheimer's disease, and Parkinson's disease.[18–23]

Despite the numerous beneficial roles that DHA potentially has been linked with, there is still a gap in the understanding of the mechanisms of action of free DHA with lipid membranes, and more specifically with those membranes found in the brain. As DHA is rapidly taken up by the brain and esterified as part of phospholipids, there have been investigations on the effect of lipid molecules containing a DHA sn–2 tail on the membrane properties. Generally, it has been found that membranes rich in DHA-esterified lipids have a decreased order due to the large number of double bonds and the rapid conversion from cis and trans of these double bonds.[24–27] This decreased order is then thought to lead to the increased permeability which has been generally observed,[28–31] as well as an increased fluidity that has been observed in model phospholipid bilayers.[29,32,33] However, in membranes extracted from animals, very little effect on the fluidity, or an increase in fluidity of the membranes

was observed when studying the effect of varying diets of the animals or supplementing the cells with DHA in culture.[31,34–38]

The effect of free DHA on membrane properties has been limited to the investigation of model PC-lipid bilayers to date. Sherratt and Mason found that DHA increases the electron density in the region of the bilayer nearer the water/membrane interface when added to a POPC and cholesterol membrane, and did not have a significant effect on the electron density measured with x-ray diffraction in the hydrophobic core.[39] More recently, Pedroni *et al.* have used a combination of experiments and all-atom molecular dynamics simulations to investigate the effect of free DHA on the structural and dynamic properties of a membrane containing 70% DPPC and 30% cholesterol. They observed that adding 30% DHA to this membrane that the lipid order within the membrane decreases to almost the same order as observed in a pure DPPC membrane, and the diffusion of lipids increase to near the same rate as observed in a pure DPPC membrane.[40]

Free protonated docosahexaenoic acid (DHAP; Figure 1) has recently been shown to modify the lipid composition in flies with Alzheimer's Disease, and as a result it was found to improve their behavioural motor function and increase their lifespan.[41] In this manuscript, we present the results of a series of all-atom molecular dynamics (MD) simulations that were used to investigate how varying concentrations of DHAP affect the structure and dynamics of a complex brain lipid membrane. In an effort towards simulating a realistic lipid bilayer, we used a healthy human brain model (BH) where the lipid composition was obtained from experiment and contains a cocktail of 26 different lipid types and ∼50% cholesterol.[42,43] In summary, our results show that incremental additions of DHAP to the BH membrane at 17%, 30% and 38% increasingly disorders the membrane packing and fluidises the membrane, whereby the shift towards larger tilt angles (i.e., greater orientational flexibility) and faster lipid dynamics facilitate the flip-flop events of DHAP.

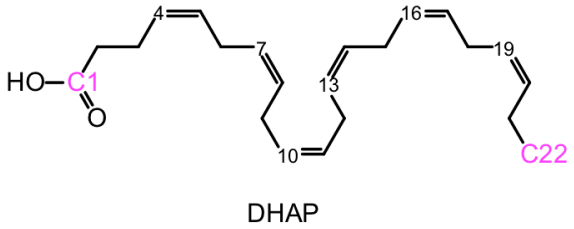

Figure 1: Chemical structure of protonated docosahexaenoic acid (DHAP).

Computational Details

Model membranes

Five heterogeneous systems were simulated in total (Table 1). The BH system uses the same composition from previous work that realistically mimics a healthy human brain cell membrane without DHAP.[43] Four other systems contained the BH membrane along with uncharged (protonated) DHAP molecules in increasing molar fractions of 17% (BH-DHAP40), 30% (BH-DHAP80), 38% (BH-DHAP120), and 50% (BH-DHAP200) (Tables 1). All lipid distributions are initially symmetric in the upper and lower leaflets. Full lipid compositions can be found in Table 2, with the corresponding general structures of the various lipid types in Figure S1. All systems were generated using the *CHARMM-GUI Membrane Builder*. The updated CHARMM36 force field was used for all lipids, and the TIP3P model was used for water.[44–46] Lipid molecules were placed at random within each leaflet at the start of the simulation. All membranes were then solvated with a water thickness of at least 22.5 Å (default setting), and neutralised to a salt concentration of 150 mM NaCl.

Table 1: System details of BH with and without DHAP. Full lipid composition of BH is given in Table 2. All lipid distributions are symmetric in the upper and lower leaflets.

Systems	BH	BH-DHAP40	BH-DHAP80	BH-DHAP120	BH-DHAP200
BH lipids per leaflet	200	200	200	200	200
DHAP per leaflet	0	40	80	120	200
Total lipids per leaflet	200	240	280	320	400
% DHAP	0%	17%	30%	38%	50%
Total waters	22,000	22,900	25,200	27,500	32,100
Total production (ns)	300	500	500	500	700

Table 2: Lipid composition per leaflet for the BH membrane, which contains a total of 26 lipid types.

BH				
Lipid Type	Resname	$sn1/sn2$	Num. Lipids	Total
CHOL	CHL1	-	98	98
PC	SDPC	18:0/22:6	3	32
	SAPC	18:0/20:4	6	
	POPC	16:0/18:1	11	
	DPPC	16:0/16:0	8	
	PLPC	16:0/22:6	4	
PE	SDPE	18:0/22:6	8	31
	SAPE	18:0/20:4	11	
	SLPE	18:0/18:2	8	
	SOPE	18:0/18:1	3	
	DSPE	18:0/18:0	1	
PS	SDPS	18:0/22:6	2	5
	SOPS	18:0/18:1	3	
PI	SAPI25	18:0/20:4	4	6
	PNPI25	16:0/18:3	1	
	POPI25	16:0/18:1	1	
SM	ASM	18:1/20:0	11	16
	NSM	18:1/24:1	5	
CER	CER180	18:1/18:0	1	12
	CER241	18:1/24:1	1	
	GALCER241	18:1/24:1	2	
	GALCER240	18:1/24:0	1	
	GLCCER200	18:1/20:0	2	
	GLCCER241	18:1/24:1	1	
	SLFCER240	18:1/24:0	2	
	SLFCER241	18:1/24:1	2	
Total				200

MD simulations

All simulations were run using GROningen MAchine for Chemical Simulations (GROMACS) version 2018.[47] The simulation protocol prescribed by CHARMM-GUI was followed,[45,46] whereby (i) initial structures were energy-minimised using steepest descent, (ii) systems were equilibrated using the NVT (constant Number of particles, Volume, and Temperature) followed by the NPT (constant Number of particles, Pressure, and Temperature) ensembles for at least 1.8 ns, and (iii) finally, MD productions were performed under NPT. Throughout, the simulation temperature was maintained at 310 K by the Nosé-Hoover thermostat,[48] at a time constant of 5 ps. Semi-isotropic pressure coupling was maintained at 1 bar by the Parrinello-Rahman barostat,[49] at a time constant of 5 ps and a standard compressibility of 4.5×10^{-5} bar^{-1}. The Verlet cut-off scheme was employed. Electrostatic interactions were calculated using the Particle-Mesh Ewald algorithm. Both electrostatic and Van der Waals interactions were cut off beyond 1.2 nm. All bonds involving hydrogen atoms were constrained using the LINCS algorithm.[50]

Data analysis details

Ensembled averages were calculated over the full length of the production trajectories. Standard errors (SE) were calculated as standard deviations of the mean. The area per lipids (APLs), lipid order parameter (S_{CH}), and lipid tilt angles were calculated using the membrane analysis tool, MEMBPLUGIN.[51] The bilayer thickness, surface roughness, difference in the distribution of DHAP between the upper and lower leaflets, finding the number of successful and aborted flip-flop events, and hydrogen bond analysis[52] were analysed using MDAnalysis.[53] The lateral diffusion and mass densities were calculated using the *gmx msd* and *gmx density* modules, respectively, from the GROMACS package.[47] Radial distribution functions ($g(r)$) were calculated using the Radial Pair Distribution Function plugin on VMD, using bin widths of 0.1 Å.[54] Visualisation images were produced using VMD.[55] All plots were generated by the Matplotlib plotting library using Python.[56] Further details regarding each

of the analyses conducted during the preparation of this manuscript are presented in the relevant parts of the Results and Discussions.

Results and Discussion

Effects of DHAP on the brain membrane structure

Equilibration of the systems in this work was assessed by the membrane thickness, surface roughness, and the average area per lipid (APL). All three parameters show successful convergence over the course of the simulations, and thus, the bilayers have reached a steady state. The membrane thickness was measured using the average phosphorus-to-phosphorus distance in the z-direction (Figure S2).[57] The surface roughness was defined using the root-mean-square deviation in the z-positions of the C2 or C2S atoms of non-CHOL lipids (Figure S3).[58] The average APL was calculated whereby the xy-area of the simulation box is divided by the number of lipids per leaflet (Figure S4), while the APL for each lipid type was calculated using the Voronoi method to account for a heterogeneous lipid mixture (Figures S5-S6).[51]

It is worth noting that the healthy human brain model (BH) naturally contains ∼50% cholesterol, and so, its physical properties in Table 3 will resemble bilayers of similar cholesterol content.[43] The BH membrane which also contains a complex mixture of 26 different lipids equilibrates to the largest bilayer thickness (47.4 Å), the smallest average roughness (0.7 Å), the largest APL on average (42.2 Å^2), and the smallest APLs for each lipid type (∼29–56 Å^2) in comparison to the other three bilayers containing DHAP (Table 3). Incremental additions of DHAP to the BH membrane in molar fractions of 17% (BH-DHAP40), 30% (BH-DHAP80), and 38% (BH-DHAP120) causes the bilayer thickness to decrease (Figure S2), the membrane's interface to become rougher (Figure S3), the average APL to decrease (Figure S4), and the APLs of each lipid type to increase (Figures S5–S6) (Table 3). The average APL decreases with greater concentrations of DHAP because the APL of DHAP

is consistently the smallest (∼29 Å^2) compared to the APLs of the other lipids in the bilayers (Table 3). Thus, a larger quantity of DHAP in the membrane decreases the average APL. Further inspection of the APLs by lipid type show a general increase in APLs with increasing DHAP in the membrane, which is demonstrated by the shift in distributions toward larger areas that is more obvious for DHAP, CHOL, PC, PE, and PS (Figure S6).

Table 3: Membrane properties (mean ± standard error) with increasing molar fractions of DHAP (% DHAP). Bilayer thickness. Average surface roughness. Average area per lipid (APL), and the APLs for each lipid type. Tilt angles (and the defining vectors) in the packing and headgroup regions.

		BH	BH-DHAP40	BH-DHAP80	BH-DHAP120
Thickness (Å)		47.4 ± 0.5	46.8 ± 0.4	46.2 ± 0.4	45.9 ± 0.4
Roughness (Å)		0.7 ± 0.1	1.0 ± 0.1	1.3 ± 0.2	1.5 ± 0.2
APL (Å^2)	Average	42.2 ± 0.5	40.6 ± 0.4	39.5 ± 0.5	38.5 ± 0.6
	DHAP	-	29.3 ± 0.9	29.8 ± 0.7	29.9 ± 0.8
	CHOL	29.7 ± 0.6	30.0 ± 0.5	30.5 ± 0.5	30.8 ± 0.5
	PC	56.2 ± 1.2	57.2 ± 1.3	58.0 ± 1.4	58.4 ± 1.4
	PE	55.7 ± 1.4	56.5 ± 1.7	57.6 ± 1.7	57.7 ± 1.8
	PS	55.4 ± 2.3	57.5 ± 2.8	57.7 ± 3.2	58.7 ± 3.5
	PI	55.6 ± 2.6	57.0 ± 2.8	58.0 ± 3.2	57.7 ± 3.7
	SM	49.8 ± 1.4	50.8 ± 1.5	50.9 ± 1.5	50.9 ± 1.7
	CER	49.5 ± 1.6	49.3 ± 1.8	49.6 ± 2.2	49.9 ± 2.2
Tilt Angle (°)					
Packing	DHAP (C22→C1)	-	22.3 ± 2.0	28.3 ± 3.1	32.7 ± 3.7
	DHAP (C11→C1)	-	22.1 ± 2.0	28.7 ± 3.1	33.1 ± 3.7
	DHAP (C22→C11)	-	37.4 ± 3.3	42.9 ± 3.4	47.0 ± 3.5
	CHOL (C17→C3)	11.3 ± 0.7	12.7 ± 0.8	13.9 ± 0.8	14.7 ± 0.9
Headgroup	PC (P→N)	65.9 ± 3.0	65.8 ± 3.2	65.2 ± 3.2	64.8 ± 3.2
	PE (P→N)	73.5 ± 2.9	73.0 ± 3.3	72.1 ± 3.3	71.5 ± 3.2
	PS (P→N)	65.3 ± 8.5	64.6 ± 8.4	66.4 ± 8.6	65.1 ± 8.8
	PI (P→C14)	52.3 ± 5.6	53.7 ± 5.2	54.3 ± 5.8	56.0 ± 5.5
	SM (P→N)	69.5 ± 4.2	69.8 ± 4.2	69.4 ± 4.3	70.1 ± 4.2
	CER (O1→C4)	41.0 ± 4.6	41.6 ± 5.0	42.1 ± 5.0	43.7 ± 5.0

In the hydrophobic region, the ordering of the lipid acyl chains was determined using

the order parameter (S_{CH}), $S_{CH} = \left\langle \frac{3\ \cos^2\ \theta - 1}{2} \right\rangle$, where θ is the angle formed by a C–H vector and the vector that is normal to the bilayer.[57] In an effort to approximate the overall order of the BH membrane, the S_{CH} was averaged across the various lipids if they contained a *sn*16:0, *sn*18:0, or *sn*22:6 acyl chain, while the *sn*22:6 chain of DHAP was calculated separately. Generally, the *sn*16:0 and *sn*18:0 chains show increasing S_{CH} values from carbons 2 to 8 due to tighter packing around the membrane interface, before decreasing towards the terminal carbons in the lipid tails where there is greater orientational flexibility nearing the membrane mid-plane (Figure 2). This trend in is in agreement with the trend in S_{CH} for the *sn*16:0 chains of DPPC in a DPPC membrane containing free DHAP, previously studied by Verde *et al.*[59] As for the *sn*22:6 chains, the numerous dips along the hydrocarbon tail is characteristic of the disordering effect of carbon-carbon double bonds (Figure 2). The S_{CH} profile for the *sn*22:6 tails within the BH lipids is consistent to those of DHAP-esterified lipids (double-tailed) from previous works,[26,60,61] and shares a similar profile to that of free DHAP (single-tailed) (Figure 2). As the molar fraction of DHAP increases in the membrane, the S_{CH} profiles show an overall decrease in order for all of the calculated acyl chains, is more significant for the *sn*16:0 and *sn*18:0 chains than for the *sn*22:6 chains (Figure 2). This shows that DHAP molecules have a disordering effect on the brain membrane considering the many double bonds within the DHAP structure. The disordering effect of DHAP appears to counter the ordering effects of cholesterol, and a steady transition of the overall membrane from a liquid-ordered state ($S_{CH} > 0.3$) to liquid-disordered state ($S_{CH} < 0.3$) is observed (Figure 2).

The lipid tilt angle is another parameter that is used to evaluate the packing environment within the bilayer. Here, we calculated the tilt angles with respect to the bilayer normal, for the steroid moiety of CHOL (C17→C3 vector, Figure S1) and the molecular alignment of DHAP (C22→C1, C11→C1, and C22→C11 vectors, Figure 1). Three vectors were used for DHAP as there are multiple double bonds in the fatty acid structure. The reported mean angles (Table 3) and the angle distributions (Figure S8) demonstrate clear shifts in

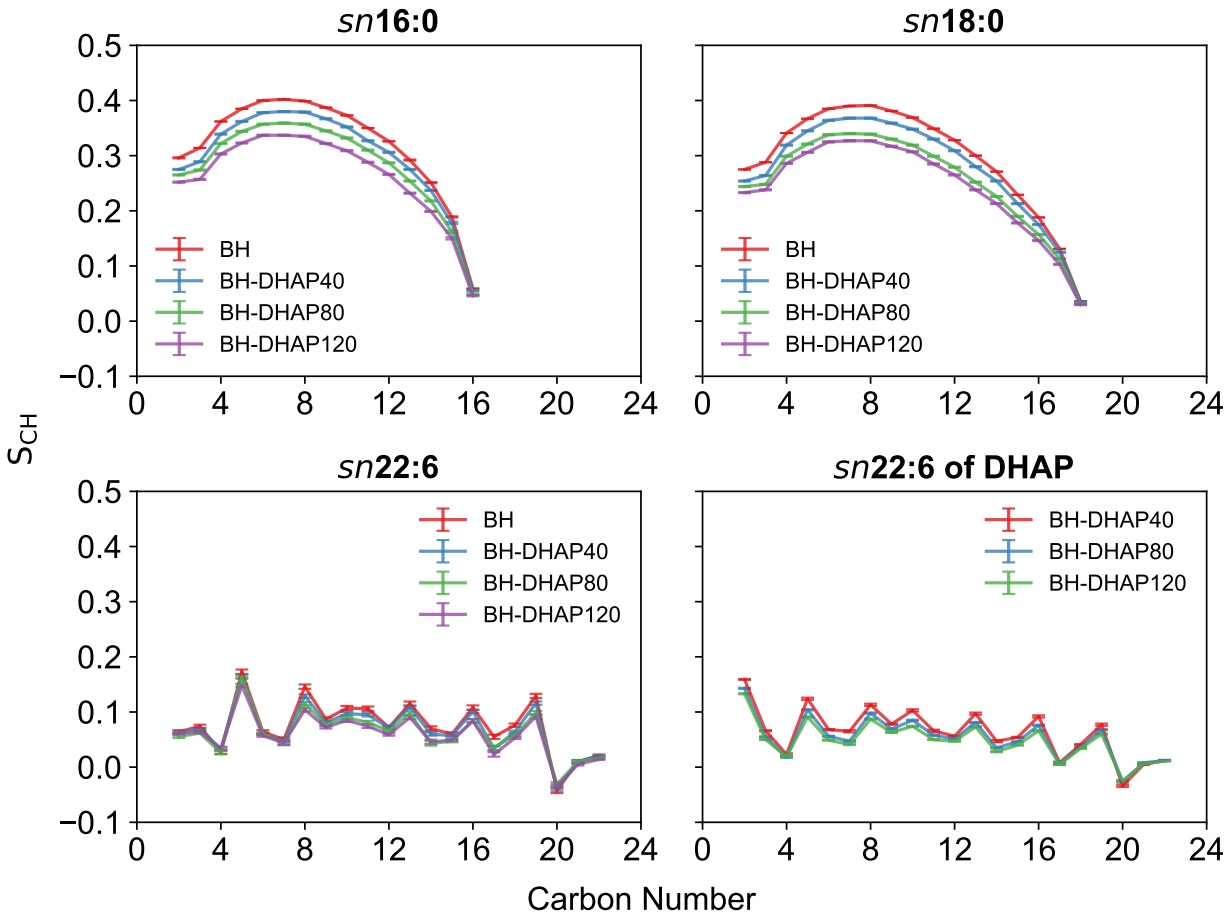

Figure 2: Order parameter profiles (S_{CH}) for the *sn*16:0, *sn*18:0, and *sn*22:6 acyl chains of lipids comprising the BH membrane, and the *sn*22:6 chain of DHAP. Standard errors for all are within $\pm$ 0.01.

orientation towards larger angles for CHOL and DHAP accompanying the molar increase of DHAP in the membrane. This implies that the membrane packing is becoming less compact, which is consistent with our results demonstrating that the lipid molecules are becoming more disordered.

The headgroup tilt angle is used to characterise the headgroup orientations of the various lipid types at the membrane interface.[57] Tilt angle distributions for the headgroups of PC, PE, PS, PI, SM, and CER lipids are broad and fairly uniform between BH, BH-DHAP40, BH-DHAP80, and BH-DHAP120 (Figure S9), indicating that the headgroup orientation is unaffected by the concentration of DHAP. Furthermore, we studied the hydration around

the carboxyl headgroup of DHAP at the membrane surface using radial distribution function ($g(r)$). As seen in Figure 3, the arrangement of water molecules (O_W atom) surrounding the C1 atom of DHAP indicate a distinct hydration shell at 3.6 Å that contains an average of 5 water molecules (Figure 3). Uniformity in the distribution across all systems similarly reinforces that the hydration of DHAP at the membrane interface is independent of the structural changes within the hydrophobic core of the bilayer as the amount of DHAP content increases (Figure 3).

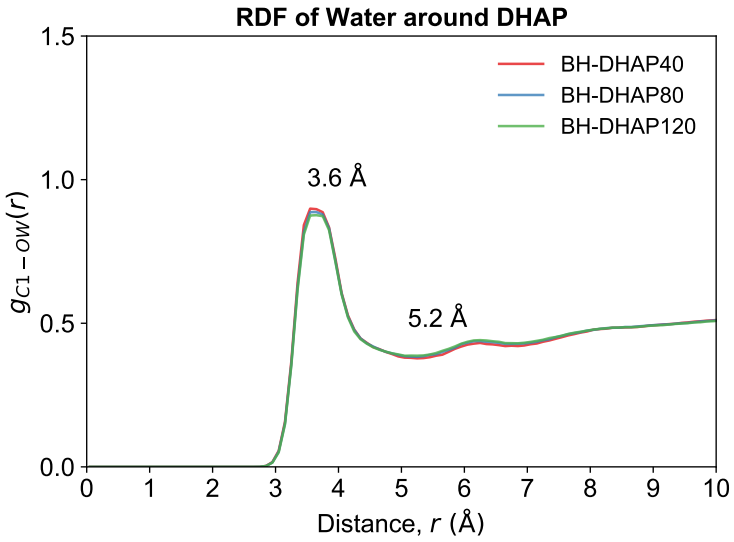

Figure 3: Radial distribution function ($g(r)$) of water molecules (O_W atom) surrounding the carboxyl headgroup (C1 atom) of DHAP. The r_{peak} averages at 3.6 Å, the r_{max} at 5.2 Å, and the coordination number at 5 water molecules.

Effects of DHAP on the brain membrane dynamics

Lateral diffusion is conventionally used to gauge the lateral movement and mixing of components (e.g., lipids, proteins, etc.) within the membrane.[57] By fitting a straight line through the values of the mean-square displacements (MSDs) as a function of lag time, the resulting gradient gives the diffusion coefficient (D) (Figure 4).[47] For bilayers that experience sub-diffusion, like in this work, the values of D obtained are anomalous.[62–65] As similarly done in previous studies,[43,64] the anomalous diffusion constants are still useful towards the

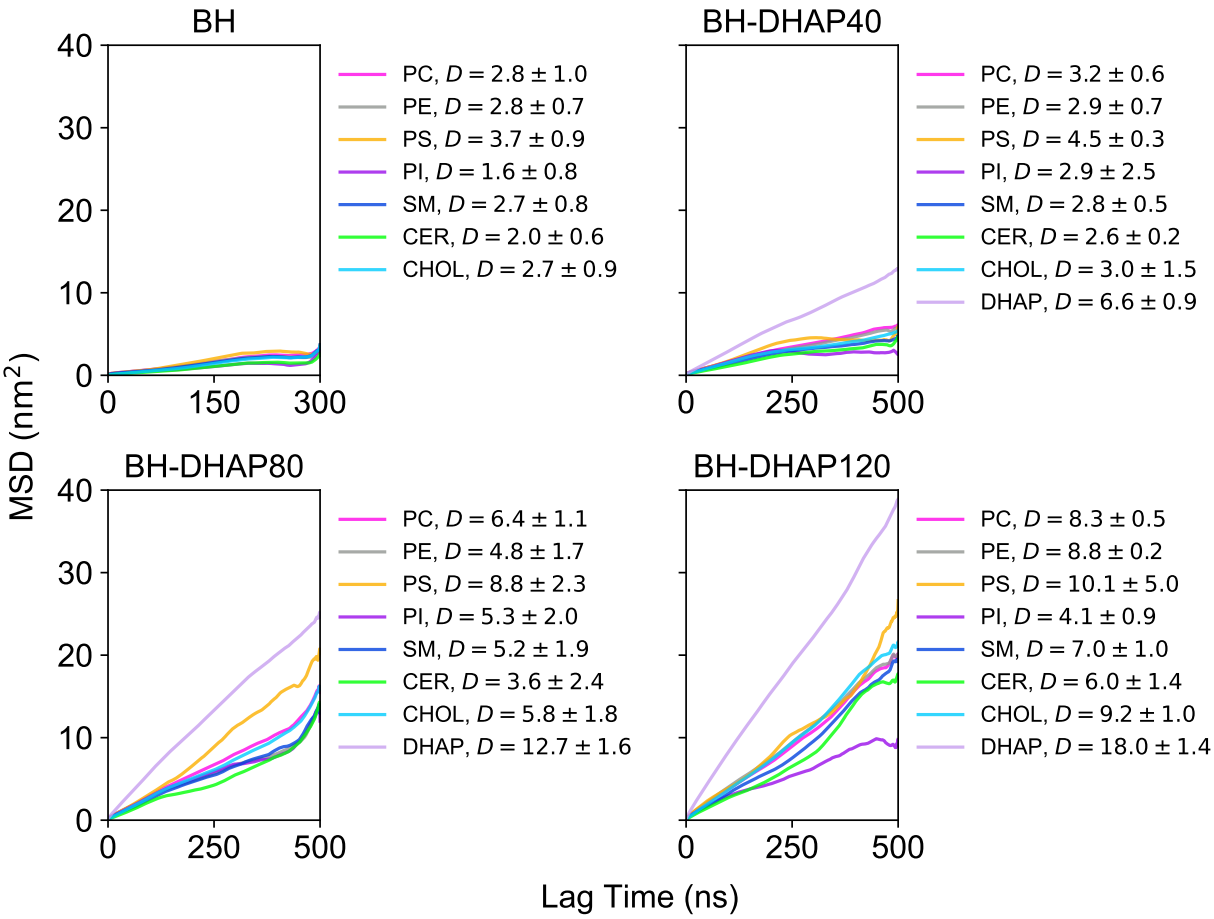

Figure 4: Mean-squared displacement (MSD) of each lipid type in the various systems as a function of lag time, and their corresponding anomalous diffusion coefficients ($D \pm$ standard error) (10^{-8} cm^2 s^{-1}).

qualitative comparison of lipid mobility between the various systems reported here. Figure 4 shows that the presence of DHAP increases the diffusion for all lipid types in the bilayer. It is worth noting that DHAP consistently has the fastest dynamics and the largest D constant compared to the other lipid species (Figure 4). Furthermore, greater amounts of DHAP in the membrane increases the values of D for each lipid type substantially (Figure 4), which means that the membrane is becoming more fluid. This result agrees with previous observations that increased unsaturation in the lipid chains, such as DHAP (and other PUFAs), increases the fluidity of model bilayers.[29,32,33,59,66] The fact that we observe an increased fluidity in the complex membranes studied in this manuscript would lend further support to

the idea that DHA increases the local fluidity even within biological membranes but it just may not be measurable with current methods.[67]

Flip-flop rates of DHAP

Numerous flip-flop events are detected for DHAP when plotting their z-positions over time (Figures S10-S12). From there, we are able to categorise a flip-flop event as either (i) **successful**: the translocation of a DHAP molecule from one leaflet to the other, or (ii) **aborted**: where a DHAP molecule attempts to flip-flop by travelling to the flip-flop range between $z \pm 8$ Å from the bilayer centre but returns to its residing leaflet eventually. Judging by the mass density profile of the C1 atom of DHAP, the flip-flop range was decided to be between $z \pm 8$ Å from the centre since the majority of DHAP are generally situated more than 8 Å away from the bilayer centre (Figure S13). We applied the machine learning technique, Density-Based Spatial Clustering of Applications with Noise (DBSCAN),[68] to identify the number of flip-flop events (N) by clustering based on a combination of time and z-positions found within the flip-flop range ($z \pm 8$ Å), where each cluster corresponds to a flip-flop event (further details in ESI; Figures S14-S22). Then, the flip-flop rate (k) can be calculated using,[69] $k = \frac{N}{t \cdot M}$, where N is the number of flip-flop events, t is the total simulation time, and M is the total number of DHAP molecules in the system (Table 4).

One of the main advantages of DBSCAN is the ability for the user to define the neighbourhood radius using the input parameter, `eps`.[68] In the ESI, we demonstrate how we have identified the value of `eps` that yielded the most accurate results for this investigation. Furthermore, there is no need to hard-code the number of clusters to find (required for algorithms, like k-means clustering, etc.), which would be highly unsuitable in this case seeing as the number of clusters can vary greatly between DHAP molecules.

As seen in Table 4, with increasing amounts of DHAP in the bilayer, the frequency of successful and aborted flip-flops also increases. It should be pointed out that the values of k for aborted flip-flops are much larger than the values of k for successful flip-flops in all

Table 4: Number of flip-flop events (N) and the corresponding flip-flop rates (k) of successful and aborted flip-flops of DHAP at increasing molar fractions of DHAP (% DHAP) in the membrane.

	BH	BH-DHAP40	BH-DHAP80	BH-DHAP120
% DHAP	0%	17%	30%	38%
Successful				
N	-	7	66	155
k (μs^{-1})	-	0.2	0.8	1.3
Aborted				
N	-	81	420	918
k (μs^{-1})	-	2.0	5.3	7.7

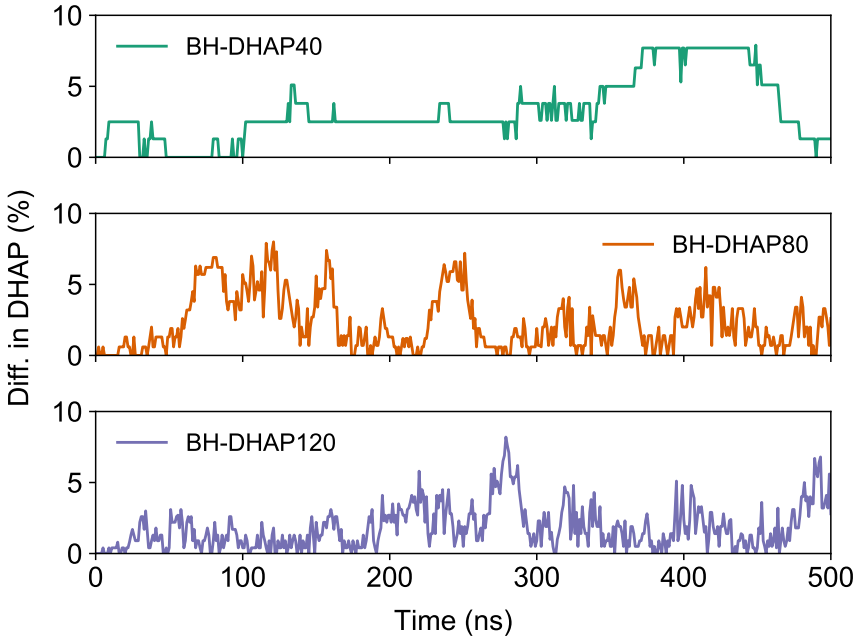

Figure 5: Difference in the number of DHAP molecules (%) between the upper leaflet ($z > 8$ Å) and lower leaflet ($z < -8$ Å) over time. The C1 atom was used as reference.

cases (Table 4). Thus, we learn that DHAP makes very frequent attempts to flip-flop, but approximately only 8% of those are successful in BH-DHAP40, 15% are successful in BH-DHAP80, and 16% are successful in BH-DHAP120, where the chances of success increases with greater concentrations of DHAP (Table 4). Hence, we also monitored the % difference in DHAP between the upper leaflet (n_{upper} at $z > +8$ Å) and lower leaflet (n_{lower} at $z < -8$ Å) over time: $\frac{|n_{upper}-n_{lower}|}{n_{upper}+n_{lower}} \times 100\%$. Interestingly, Figure 5 reveals that there is an ongoing

imbalance in the distribution of DHAP between the leaflets over time, ergo, the continuous flip-flopping of DHAP in each system is evolving what was initially a symmetric bilayer into a slightly asymmetric one.

The increasing amounts of DHAP also seems to correlate to a higher number of aborted flip-flops of another lipid, CHOL (Table S1). However, although the rates for successful flip-flop of CHOL, which has previously been reported to occur on sub-microsecond timescales,[70] are very small across all systems, translocation did occur as much as 4 times in BH-DHAP80 and 1 time in BH-DHAP120 (Table S1).

Based on the combination of analyses in terms of order parameter, lateral diffusion, and tilt angle calculations, we have observed that a less ordered membrane allows for greater membrane fluidity, which translates to a larger tilt angle, where a more flexible orientation as well as faster dynamics facilitate the flip-flop of DHAP and CHOL lipids.

Flip-flop process of DHAP

While DHAP is in the process of flip-flop within the flip-flop range at $z \pm 8$ Å from the centre, we thought it would be interesting to investigate the flip-flop duration ($\Delta t = t_{fin} - t_{ini}$), the flip-flop distance travelled in the xy-direction ($\Delta xy = \sqrt{(x_{fin} - x_{ini})^2 + (y_{fin} - y_{ini})^2}$), and the tilt angles during flip-flop (C22→C1 vector, Figure 1). The resulting distributions in Figures 6a-6d include data for both the successful and aborted flip-flops of DHAP.

Figure 6a shows that the duration of flip-flop can occur over a wide range of times. However, the distribution indicates that most flip-flops take place very rapidly, at a modal value of 1 ns or less across all systems (Figure 6a). Interestingly, some DHAP molecules can take longer to flip-flop with increasing amounts of DHAP in the membrane, up to ∼95 ns in BH-DHAP40, ∼110 ns in BH-DHAP80, and ∼150 ns in BH-DHAP120 (Figure 6a). By revisiting the z-positions of DHAP over time, the duration of some flip-flops are lengthy because some tended to linger at the bilayer centre before the flip-flop is either successful or aborted (Figures S10-S12). The flip-flop distance travelled in the xy-dimensions is less

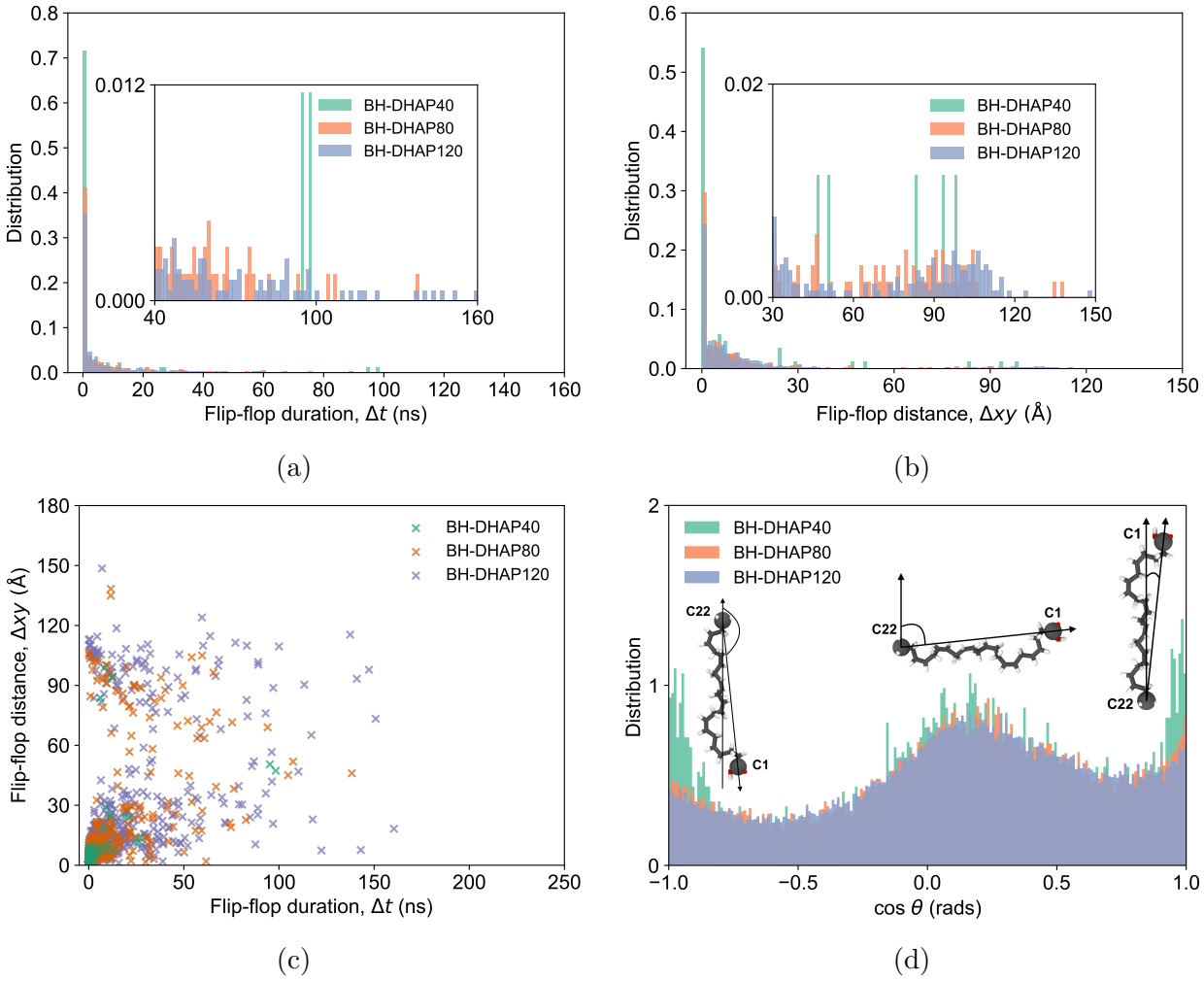

Figure 6: Distributions of the (a) flip-flop duration and (b) flip-flop distance of DHAP. (c) The flip-flop distance as a function of flip-flop duration. (d) Distribution of tilt angles of DHAP molecules that are in the process of flip-flop. All plots include events for successful and aborted flip-flops of DHAP.

studied in literature. According to Figure 6b, most DHAP molecules do not travel beyond 1 Å, but in some cases can travel over a range of distances, as far as up to 135 Å. Intriguingly, the flip-flop distance and flip-flop duration are uncorrelated, e.g., a DHAP molecule can take a wide range of times (ranging from 10–160 ns) to travel a distance of ∼20 Å during flip-flop (Figure 6c).

DHAP adopts a wide range of molecular conformations during flip-flop (Figure 6d). In all systems, the DHAP molecules exist predominantly in three conformations: parallel to the bilayer normal ($\cos\theta \approx 1.0$), anti-parallel to the normal ($\cos\theta \approx -1.0$), and perpendicular

to the normal ($\cos\theta \approx 0.2$) (Figure 6d). These three conformations are relatively equally distributed in the BH-DHAP40 system, although in BH-DHAP80 and BH-DHAP120, slightly less are found in the anti-parallel fashion ($\cos\theta \approx -1.0$). In essence, DHAP has great flexibility when near the bilayer mid-plane and is constantly re-arranging itself until it either finds a favourable position to make a successful flip-flop, or abort the flip-flop altogether.

DHAP double flip-flops and assisted flip-flops

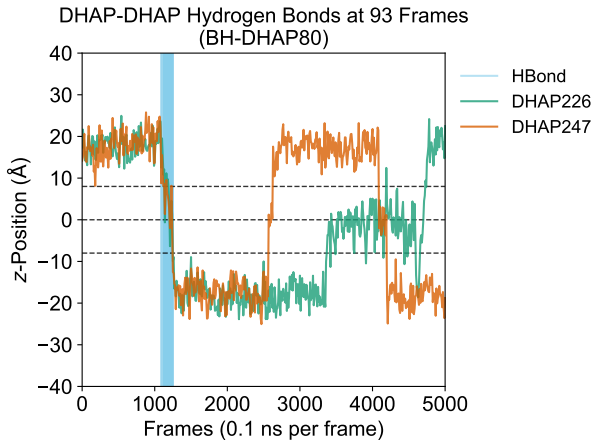

(a) Successful double flip-flop

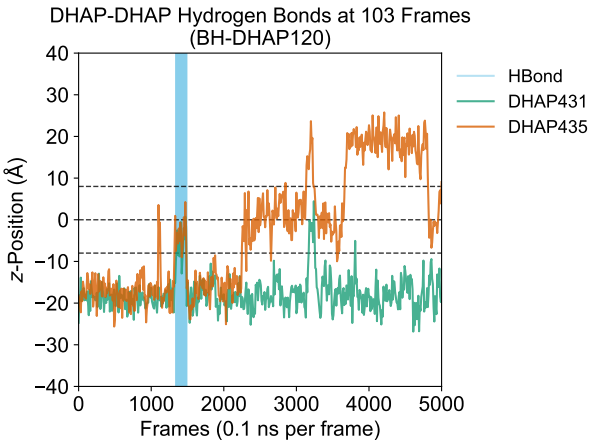

(b) Aborted double flip-flop

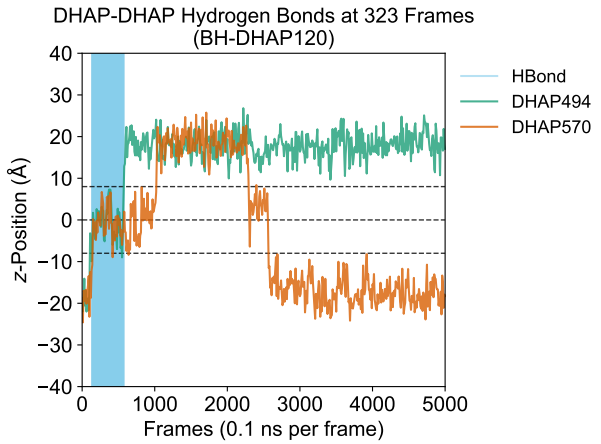

(c) Assisted flip-flop

Figure 7: The z-positions show pairs of DHAP molecules where the (a) double flip-flop is successful, (b) double flip-flop is aborted, and (c) the flip-flop is assisted by one of the DHAPs. Hydrogen bonding occurs at frames highlighted in *blue*. The C1 atom is used as reference. The bilayer is centred at $z = 0$. Hydrogen bonds between DHAP-DHAP were searched within the flip-flop range at $z \pm 8$ Å (dotted lines).

Since DHAP has a carboxyl headgroup, we were interested to see if they would hydrogen bond with each other within the flip-flop range at $z \pm 8$ Å. Indeed, instances of DHAP-DHAP hydrogen bonding increases with larger molar fractions of DHAP in the membrane. During the 500 ns simulations, we observed a total of 7 hydrogen-bonded DHAP pairs in BH-DHAP40, 322 pairs in BH-DHAP80, and 1242 pairs in BH-DHAP120. The average hydrogen bond distance ($\mathrm{HO}\cdots\mathrm{H}$) is 2.7 ± 0.1 Å, and the average bond angle ($\angle \mathrm{H}-\mathrm{O}\cdots\mathrm{H}$) is $164° \pm 7°$. By plotting the time frames at which hydrogen bonding occurs against the z-positions of DHAP over time, we were able to detect two distinct phenomena where pairs of DHAP molecules occasionally make a successful double flip-flop or an assisted flip-flop involving hydrogen bonds (Figure 7).

A successful double flip-flop describes two DHAP molecules translocating to the opposing leaflet in concert while the hydrogen bond is maintained (Figure 7a). Successful double flip-flops took place for a total of 5 DHAP-DHAP pairs in BH-DHAP80 (Figure S23), 2 pairs in BH-DHAP120 (Figure S24), and none in BH-DHAP40. Wei and Pohorille have similarly reported events of double flip-flop between two oleic acid molecules (omega-9 fatty acid, *sn*18:1) interacting via hydrogen bonds.[69] Alternatively, there are also cases of double flip-flops which were aborted, we observed 3 pairs in BH-DHAP40, 23 pairs in BH-DHAP80, and 21 pairs in BH-DHAP120 (Figures 7b & S25). It is worth noting that the duration for double flip-flops (successful and/or aborted) can take less than 1 ns, or span up to ∼87 ns.

In the cases of assisted flip-flop, two DHAPs are hydrogen bonded, but when the hydrogen bond is broken, only one of the DHAP translocates successfully to the opposing leaflet, while the other becomes free to move at random (e.g., return immediately to the resident leaflet, or diffuse in the bilayer mid-plane for a time, etc.) (Figures 7c & S26). We observed 10 assisted flip-flops in BH-DHAP80, and 11 in BH-DHAP120.

Conclusions

In this work, atomistic MD simulations were used to investigate the effects of free DHAP in a complex human brain cell membrane, in incremental molar fractions of 0% (BH), 17% (BH-DHAP40), 30% (BH-DHAP80), and 38% (BH-DHAP120). The BH bilayer mimics the prefrontal cortex cells obtained from healthy patients, which incorporates a cocktail of 26 lipid types, and is therefore a relatively realistic model. In terms of membrane physical properties, the increasing amounts of DHAP most notably affects the lipid packing, where greater disorder is observed within the membranes with increasing amounts of DHAP in the membrane. Therefore, when there is little DHAP present the membranes are in the liquid-ordered state, but when there is increasing amounts of DHAP present the membranes are in the liquid-disordered state. In terms of dynamics, the increase in the amount of DHAP has prominent effects on the lateral diffusion of lipids, where the enhanced membrane fluidity can influence the mechanisms of permeation. The ability to improve membrane permeability to the likes of drugs, small molecules, etc., could prove useful in the processes of drug design.[71,72]

The transport of polyunsaturated fatty acids into the brain is essential as they play key roles in signalling, energy production and structure of the lipid membranes, but they are not synthesised in the brain. One method of transport across the blood-brain barrier (BBB) is thought to be the passive diffusion through the lipid bilayers.[69] In particular, it has been proposed that free DHAP flip-flops across the lipid membranes that make up the BBB and deliver protons across the bilayer while doing so.[73] These flip-flop events have been been measured experimentally for a variety of PUFAs.[74,75]

For the first time to our knowledge, we have observed numerous flip-flop events of DHAP during the 500 ns trajectories in each system. We applied novel use of the machine learning technique, DBSCAN, which effectively identified flip-flop events by way of clustering. The results show that the flip-flop rates of DHAP for aborted events are exponentially larger than for successful ones, where both events increase with greater fractions of DHAP in the membrane. The flip-flop rates (k) for successful events increase in the order of

0.2 μs^{-1} (17% DHAP) < 0.8 μs^{-1} (30% DHAP) < 1.3 μs^{-1} (38% DHAP). This further supports that fatty acids, including DHAP, can diffuse directly through membranes without the help of transport proteins.

While DHAP is in the process of flip-flop, most flip-flops (aborted and/or successful) are ultimately very short in time duration ($\leq$ 0.1 ns) and very small in the xy-distance travelled ($\leq$ 1 Å). But interestingly, some can also occur over a wide range of time-lengths, distances, and tilt angles. Additionally, we noted the role of hydrogen bonds between DHAP pairs that give rise to two distinct coordinated flip-flop phenomena: double flip-flop and assisted flip-flop.

In summary, free protonated DHAP induces numerous changes in a lipid bilayer. Therefore, understanding how DHAP modifies the properties and permeability of a bilayer will add insight into the prevention methods as well as development of therapeutic remedies to target detriments associated with low level DHAP (dementia, Alzheimer's disease, Parkinson's disease, poor vision, etc.).[59,76]

Supporting Information Available

Full lipid compositions for each system, chemical structure of lipids, membrane thickness, surface roughness, average APL, APLs of each lipid type, snapshots of the BH-DHAP200 system over time, tilt angle distributions, z-positions of DHAP over time, mass densities, examples of clustering using DBSCAN, z-positions of CHOL over time, flip-flop rates of CHOL.

Acknowledgement

We are grateful for the computational support provided by the UK's HEC Materials Chemistry Consortium (funded by the EPSRC EP/L000202, EP/R029431, EP/T022213) that has allowed us to use the ARCHER UK National Supercomputing Service (http://www.archer.

ac.uk) and the UK Materials and Molecular Modelling Hub, which is partially funded by the EPSRC for THOMAS (EP/P020194) and for YOUNG (EP/T022213) to carry out the MD simulations reported in this manuscript.

References

(1) Layé, S.; Nadjar, A.; Joffre, C.; Bazinet, R. P. Anti-inflammatory effects of omega–3 fatty acids in the brain: Physiological mechanisms and relevance to pharmacology. *Pharmacol. Rev.* **2018**, *70*, 12 – 38.

(2) Lozada, L. E.; Desai, A.; Kevala, K.; Lee, J. W.; Kim, H. Y. Perinatal brain docosahexaenoic acid concentration has a lasting impact on cognition in mice. *J. Nutr.* **2017**, *147*, 1624 – 1630.

(3) Cao, D.; Kevala, K.; Kim, J.; Moon, H. S.; Jun, S. B.; Lovinger, D.; Kim, H. Y. Docosahexaenoic acid promotes hippocampal neuronal development and synaptic function. *J. Neurochem.* **2009**, *111*, 510 – 521.

(4) Söderberg, M.; Edlund, C.; Kristensson, K.; Dallner, G. Fatty acid composition of brain phospholipids in aging and in Alzheimer's disease. *Lipids* **1991**, *26*, 421–425.

(5) Das, U. N. Essential fatty acids: Biochemistry, physiology and pathology. *Biotechnol. J.* **2006**, *1*, 420 – 439.

(6) Blasbalg, T. L.; Hibbeln, J. R.; Ramsden, C. E.; Majchrzak, S. F.; Rawlings, R. R. Changes in consumption of omega–3 and omega–6 fatty acids in the United States during the 20th century. *Am. J. Clin. Nutr.* **2011**, *93*, 950 – 962.

(7) Bradbury, J. Docosahexaenoic acid (DHA): An ancient nutrient for the modern human brain. *Nutrients* **2011**, *3*, 529–554.

(8) Calder, P. C. Marine omega–3 fatty acids and inflammatory processes: Effects, mechanisms and clinical relevance. *Biochim. Biophys. Acta* **2015**, *1851*, 469 – 484.

(9) Mozaffarian, D.; Wu, J. H. Y. (n–3) fatty acids and cardiovascular health: Are effects of EPA and DHA shared or complementary? *J. Nutr.* **2012**, *142*, 614S – 625S.

(10) Asztalos, I. B.; Gleason, J. A.; Sever, S.; Gedik, R.; Asztalos, B. F.; Horvath, K. V.; Dansinger, M. L.; Lamon-Fava, S.; Schaefer, E. J. Effects of eicosapentaenoic acid and docosahexaenoic acid on cardiovascular disease risk factors: A randomized clinical trial. *Metabolism* **2016**, *65*, 1636 – 1645.

(11) Laidlaw, M.; Cockerline, C. A.; Rowe, W. J. A randomized clinical trial to determine the efficacy of manufacturers recommended doses of omega–3 fatty acids from different sources in facilitating cardiovascular disease risk reduction. *Lipids Health Dis.* **2014**, *13*, 99.

(12) Kromhout, D.; Giltay, E. J.; Geleijnse, J. M. n–3 fatty acids and cardiovascular events after myocardial infarction. *N. Engl. J. Med.* **2010**, *363*, 2015 – 2026.

(13) de Luis, D.; Domingo, J. C.; Izaola, O.; Casanueva, F. F.; Bellido, D.; Sajoux, I. Effect of DHA supplementation in a very low-calorie ketogenic diet in the treatment of obesity: A randomized clinical trial. *Endocrine* **2016**, *54*, 111 – 122.

(14) Allaire, J.; Couture, P.; Leclerc, M.; Charest, A.; Marin, J.; Lépine, M.; Talbot, D.; Tchernof, A.; Lamarche, B. A randomized, crossover, head-to-head comparison of eicosapentaenoic acid and docosahexaenoic acid supplementation to reduce inflammation markers in men and women: The comparing EPA to DHA (ComparED) study. *Am. J. Clin. Nutr.* **2016**, *104*, 280 – 287.

(15) Das, U. N. Bioactive lipids in COVID–19 – Further evidence. *Biochim. Biophys. Acta* **2021**, *52*, 107 – 120.

(16) Rogero, M. M.; Leão, M. C.; Santana, T. M.; Pimentel, M. V. M. B.; Carlini, G. C. G.; da Silveira, T. F. F.; Gonçalves, R. C.; Castro, L. C. Potential benefits and risks of omega–3 fatty acids supplementation to patients with COVID–19. *Free Radic. Biol. Med.* **2021**, *156*, 190 – 199.

(17) Innis, S. M. Dietary (n–3) fatty acids and brain development. *J. Nutr.* **2007**, *137*, 855 – 859.

(18) Hachem, M.; Belkouch, M.; Lo Van, A.; Picq, M.; Bernoud-Hubac, N.; Lagarde, M. Brain targeting with docosahexaenoic acid as a prospective therapy for neurodegenerative diseases and its passage across blood brain barrier. *Biochimie* **2020**, *170*, 203 – 211.

(19) Lukiw, W. J.; Bazan, N. G. Docosahexaenoic acid and the aging brain. *J. Nutr.* **2008**, *138*, 2510 – 2514.

(20) Gao, X.; Chen, H.; Fung, T. T.; Logroscino, G.; Schwarzschild, M. A.; Hu, F. B.; Ascherio, A. Prospective study of dietary pattern and risk of Parkinson disease. *Am. J. Clin. Nutr.* **2007**, *86*, 1486 – 1494.

(21) Hashimoto, M.; Hossain, S.; Al Mamun, A.; Matsuzaki, K.; Arai, H. Docosahexaenoic acid: One molecule diverse functions. *Crit. Rev. Biotechnol.* **2017**, *37*, 579 – 597.

(22) Cole, G. M.; Ma, Q. L.; Frautschy, S. A. Omega–3 fatty acids and dementia. *Prostaglandins Leukot. Essent. Fat. Acids* **2009**, *81*, 213 – 221.

(23) Cole, G. M.; Frautschy, S. A. DHA may prevent age-related dementia. *J. Nutr.* **2010**, *140*, 869 – 874.

(24) Saiz, L.; Klein, M. L. Structural properties of a highly polyunsaturated lipid bilayer from molecular dynamics simulations. *Biophys. J.* **2001**, *81*, 204 – 216.

(25) Huber, T.; Rajamoorthi, K.; Kurze, V. F.; Beyer, K.; Brown, M. F. Structure of docosahexaenoic acid-containing phospholipid bilayers as studied by ^{2}H NMR and molecular dynamics simulations. *J. Am. Chem. Soc.* **2002**, *124*, 298 – 309.

(26) Feller, S. E.; Gawrisch, K.; Mackerell, A. D. Polyunsaturated fatty acids in lipid bilayers: intrinsic and environmental contributions to their unique physical properties. *J. Am. Chem. Soc.* **2002**, *124*, 318–326.

(27) Feller, S. E.; Gaweisch, K.; Woolf, T. B. Rhodopsin exhibits a preference for solvation by polyunsaturated docosahexaenoic acid. *J. Am. Chem. Soc.* **2003**, *125*, 4434 – 4435.

(28) Huster, D.; Arnold, K.; Gawrisch, K. Influence of docosahexaenoic acid and cholesterol on lateral lipid organization in phospholipid mixtures. *Biochem.* **1998**, *37*, 17299 – 17308.

(29) Mitchell, D. C.; Litman, B. J. Effect of cholesterol on molecular order and dynamics in highly polyunsaturated phospholipid bilayers. *Biophys. J.* **1998**, *75*, 896 – 908.

(30) Holte, L. L.; Peter, S. A.; Sinnwell, T. M.; Gawrisch, K. ^{2}H nuclear magnetic resonance order profiles suggest a change of molecular shape for phosphatidylcholines containing a polyunsaturated acyl chain. *Biophys. J.* **1995**, *68*, 2396 – 2403.

(31) Stillwell, W.; Jenski, L. J.; Crump, F. T.; Ehringer, W. Effect of docosahexaenoic acid on mouse mitochondrial membrane properties. *Lipids* **1997**, *32*, 497 – 506.

(32) Salem Jr., N.; Niebylski, C. D. The nervous system has an absolute molecular species requirement for proper function. *Mol. Membr. Biol.* **1995**, *12*, 131 – 134.

(33) Mitchell, D. C.; Litman, B. J. Molecular order and dynamics in bilayers consisting of highly polyunsaturated phospholipids. *Biophys. J.* **1998**, *74*, 879 – 891.

(34) Wahnon, R.; Cogan, U.; Mokady, S. Dietary fish oil modulates the alkaline phosphatase

activity and not the fluidity of rat intestinal microvillus membrane. *J. Nutr.* **1992**, *122*, 1077 – 1084.

(35) Yorek, M.; Leeney, E.; Dunlap, J.; Ginsberg, B. Effect of fatty acid composition on insulin and IGF-I binding in retinoblastoma cells. *Invest. Ophthalmol. Vis. Sci.* **1989**, *30*, 2087 – 2092.

(36) Sobajima, T.; Tamiya-Koizumi, K.; Ishihara, H.; Kojima, K. Effects of fatty acid modification of ascites tumor cells on pulmonary metastasis in rat. *Jpn. J. Cancer Res.* **1986**, *77*, 657 – 663.

(37) Clamp, A. G.; Ladha, S.; Clark, D. C.; Grimble, R. F.; Lund, E. K. The influence of dietary lipids on the composition and membrane fluidity of rat hepatocyte plasma membranes. *Lipids* **1997**, *32*, 179 – 184.

(38) Brown, E. R.; Subbaiah, P. V. Differential effects of eicosapentaenoic acid and docosahexaenoic acid on human skin fibroblasts. *Lipids* **1994**, *29*, 825 – 829.

(39) Scherratt, S. C. R.; Mason, R. P. Eicosapentaenoic acid and docosahexaenoic acid have distinct membrane locations and lipid interactions as determined by X-ray diffraction. *Chem. Phys. Lipids* **2018**, *212*, 73 – 79.

(40) Pedroni, V. I.; Sierra, M. B.; Alarcòn, L. M.; Verde, A. R.; Appignanesi, G. A.; Morini, M. A. A certain proportion of docosahexaenoic acid tends to revert structural and dynamical effects of cholesterol on lipid membranes. *Biochim. Biophys. Acta Biomembr.* **2021**, *1863*, 183584.

(41) Mohaibes, R. J.; Fiol-deRoque, M. A.; Torres, M.; Ordinas, M.; Lòpez, D. J.; Castro, J. A.; Escribà, P. V.; Busquets, X. The hydroxylated form of docosahexaenoic acid (DHA-H) modifies the brain lipid composition in a model of Alzheimer's disease, improving behavioral motor function and survival. *Biochim. Biophys. Acta* **2017**, *1859*, 1596 – 1603.

(42) Chan, R. B.; Oliveira, T. G.; Cortes, E. P.; Honig, L. S.; Duff, K. E.; Small, S. A.; Wenk, M. R.; Shui, G.; Di Paolo, G. Comparative lipidomic analysis of mouse and human brain with Alzheimer disease. *J. Biol. Chem.* **2012**, *287*, 2678–88.

(43) Yee, S. M.; Gillams, R. J.; McLain, S. E.; Lorenz, C. D. Effects of lipid heterogeneity on model human brain lipid membranes. *Soft Matter* **2021**, *17*, 126–135.

(44) Wu, E. L.; Cheng, X.; Jo, S.; Rui, H.; Song, K. C.; Dávila-Contreras, E. M.; Qi, Y.; Lee, J.; Monje-Galvan, V.; Venable, R. M. et al. CHARMM-GUI membrane builder toward realistic biological membrane simulations. *J. Comput. Chem.* **2014**, *35*, 1997–2004.

(45) Lee, J.; Cheng, X.; Swails, J. M.; Yeom, M. S.; Eastman, P. K.; Lemkul, J. A.; Wei, S.; Buckner, J.; Jeong, J. C.; Qi, Y. et al. CHARMM-GUI input generator for NAMD, GROMACS, AMBER, OpenMM, and CHARMM/OpenMM simulations using the CHARMM36 additive force field. *J. Chem. Theory Comput.* **2016**, *12*, 405–413.

(46) Lee, J.; Patel, D. S.; Støahle, J.; Park, S.-J.; Kern, N. R.; Kim, S.; Lee, J.; Cheng, X.; Valvano, M. A.; Holst, O. et al. CHARMM–GUI membrane builder for complex biological membrane simulations with glycolipids and lipoglycans. *J. Chem. Theory Comput.* **2019**, *15*, 775–786.

(47) Van der Spoel, D.; Hess, B. GROMACS–The road ahead. *Wiley Interdiscip. Rev. Comput. Mol. Sci.* **2011**, *1*, 710–715.

(48) Evans, D. J.; Holian, B. L. The Nose-Hoover thermostat. *J. Chem. Phys.* **1985**, *83*, 4069–4074.

(49) Parrinello, M.; Rahman, A. Polymorphic transitions in single crystals: A new molecular dynamics method. *J. Appl. Phys.* **1981**, *52*, 7182–7190.

(50) Hess, B.; Bekker, H.; Berendsen, H. J.; Fraaije, J. G. LINCS: A linear constraint solver for molecular simulations. *J. Comput. Chem.* **1997**, *18*, 1463–1472.

(51) Guixà-González, R.; Rodriguez-Espigares, I.; Ramírez-Anguita, J. M.; Carrió-Gaspar, P.; Martinez-Seara, H.; Giorgino, T.; Selent, J. MEMBPLUGIN: Studying membrane complexity in VMD. *Bioinformatics* **2014**, *30*, 1478–1480.

(52) Smith, P.; Ziolek, R. M.; Gazzarrini, E.; Owen, D. M.; Lorenz, C. D. On the interaction of hyaluronic acid with synovial fluid lipid membranes. *Phys. Chem. Chem. Phys.* **2019**, *21*, 9845–9857.

(53) Michaud-Agrawal, N.; Denning, E. J.; Woolf, T. B.; Oliver, B. MDAnalysis: A toolkit for the analysis of molecular dynamics simulations. *J. Comput. Chem.* **2011**, *32*, 2319–2327.

(54) Levine, B. G.; Stone, J. E.; Kohlmeyer, A. Fast analysis of molecular dynamics trajectories with graphics processing units-radial distribution function histogramming. *J. Comput. Phys.* **2011**, *230*, 3556–3569.

(55) Humphrey, W.; Dalke, A.; Schulten, K. VMD: Visual molecular dynamics. *J. Mol. Graph.* **1996**, *14*, 33–8.

(56) Hunter, J. D. Matplotlib: A 2D graphics environment. *Comput. Sci. Eng.* **2007**, *9*, 90–95.

(57) Moradi, S.; Nowroozi, A.; Shahlaei, M. Shedding light on the structural properties of lipid bilayers using molecular dynamics simulation: A review study. *RSC Adv.* **2019**, *9*, 4644–4658.

(58) Plesnar, E.; Subczynski, W. K.; Pasenkiewicz-Gierula, M. Saturation with cholesterol increases vertical order and smoothes the surface of the phosphatidylcholine bilayer: A molecular simulation study. *Biochim. Biophys. Acta, Biomembr.* **2012**, *1818*, 520–529.

(59) Verde, A.; Sierra, M.; Alarcón, L.; Pedroni, V.; Appignanesi, G.; Morini, M. Experimental and computational studies of the effects of free DHA on a model phosphatidylcholine membrane. *Chem. Phys. Lipids* **2018**, *217*, 12–18.

(60) Leng, X.; Kinnun, J. J.; Cavazos, A. T.; Canner, S. W.; Shaikh, S. R.; Feller, S. E.; Wassall, S. R. All n-3 PUFA are not the same: MD simulations reveal differences in membrane organization for EPA, DHA and DPA. *Biochim. Biophys. Acta Biomembr.* **2018**, *1860*, 1125–1134.

(61) Gawrisch, K.; Eldho, N. V.; Holte, L. L. The structure of DHA in phospholipid membranes. *Lipids* **2003**, *38*, 445–452.

(62) Javanainen, M.; Hammaren, H.; Monticelli, L.; Jeon, J.-H.; Miettinen, M. S.; Martinez-Seara, H.; Metzler, R.; Vattulainen, I. Anomalous and normal diffusion of proteins and lipids in crowded lipid membranes. *Faraday Discuss.* **2013**, *161*, 397–417.

(63) Kneller, G. R.; Baczynski, K.; Pasenkiewicz-Gierula, M. Consistent picture of lateral subdiffusion in lipid bilayers: Molecular dynamics simulation and exact results. *J. Chem. Phys* **2011**, *135*, 141105.

(64) Plesnar, E.; Subczynski, W. K.; Pasenkiewicz-Gierula, M. Comparative computer simulation study of cholesterol in hydrated unary and binary lipid bilayers and in an anhydrous crystal. *J. Phys. Chem. B.* **2013**, *117*, 8758–69.

(65) Domicevica, L.; Koldsø, H.; Biggin, P. C. Multiscale molecular dynamics simulations of lipid interactions with P-glycoprotein in a complex membrane. *J. Mol. Graph. Model.* **2018**, *80*, 147–156.

(66) Javanainen, M.; Martinez-Seara, H. Rapid diffusion of cholesterol along polyunsaturated membranes via deep dives. *Phys. Chem. Chem. Phys.* **2019**, *21*, 11660.

(67) Stillwell, W.; Wassall, S. R. Docosahexaenoic acid: Membrane properties of a unique fatty acid. *Chemistry and Physics of Lipids* **2003**, *126*, 1–27.

(68) Pedregosa, F.; Varoquaux, G.; Gramfort, A.; Michel, V.; Thirion, B.; Grisel, O.; Blondel, M.; Prettenhofer, P.; Weiss, R.; Dubourg, V. et al. Scikit-learn: Machine learning in Python. *J. Mach. Learn. Res.* **2011**, *12*, 2825–2830.

(69) Wei, C.; Pohorille, A. Flip-flop of oleic acid in a phospholipid membrane: Rate and mechanism. *J. Phys. Chem. B.* **2014**, *118*, 12919–12926.

(70) Drew Bennett, W. F.; Maccallum, J. L.; Hinner, M. J.; Marrink, S. J.; Tieleman, D. P. Molecular view of cholesterol flip-flop and chemical potential in different membrane environments. *J. Am. Chem. Soc.* **2009**, *131*, 12714–12720.

(71) Shaitan, K. V.; Antonov, M. Y.; Tourleigh, Y. V.; Levtsova, O. V.; Tereshkina, K. B.; Nikolaev, I. N.; Kirpichnikov, M. P. Comparative study of molecular dynamics, diffusion, and permeability for ligands in biomembranes of different lipid composition. *Biochem. (Mosc.) Suppl. Ser. A Membr. Cell Biol.* **2008**, *2*, 73–81.

(72) Mitragotri, S. Modeling skin permeability to hydrophilic and hydrophobic solutes based on four permeation pathways. *J. Control. Release* **2003**, *86*, 69–92.

(73) Hamilton, J. A.; Brunaldi, K. A model for fatty acid transport into the brain. *J. Mol. Neurosci.* **2007**, *33*, 12 – 17.

(74) Kamp, F.; Zakim, D.; Zhang, F.; Noy, N.; Hamilton, J. A. Fatty acid flip–flop in phospholipid bilayers is extremely fast. *Biochem.* **1995**, *34*, 11928 – 11937.

(75) Kleinfeld, A. M.; Chu, P.; Romero, C. Transport of long-chain native fatty acids across lipid bilayer membranes indicates that transbilayer flip-flop is rate limiting. *Biochem.* **1997**, *36*, 14146 – 14158.

(76) Schaefer, E. J.; Bongard, V.; Beiser, A. S.; Lamon-Fava, S.; Robins, S. J.; Au, R.; Tucker, K. L.; Kyle, D. J.; Wilson, P. W. F.; Wolf, P. A. Plasma phosphatidylcholine docosahexaenoic acid content and risk of dementia and Alzheimer disease. *Arch. Neurol* . **2006**, *63*, 1545–1550.